



Role of rGO on mechanical, thermal, and piezoelectric behaviour of PVDF-BTO nanocomposites for energy harvesting applications

Nikhil Dilip Kulkarni¹ · Poonam Kumari¹

Received: 11 November 2022 / Accepted: 5 January 2023 / Published online: 23 January 2023
© The Polymer Society, Taipei 2023

Abstract

The low-cost and highly flexible piezoelectric nanogenerators (PENGs) have potential applications in mechanical energy harvesting and low power electronics. The low piezo response of PVDF limits its use in commercial sensory applications. In this work, a Polyvinylidene fluoride (PVDF) is reinforced with fixed quantity of Barium titanate (BTO) and varying concentrations of reduced graphene oxide (rGO) to enhance piezoelectric behaviour of PVDF films. Effect of higher rGO reinforcement (over 0.45 wt%) on PVDF-BTO composite energy harvesting performance was studied for the first time using solvent casting approach followed by electrode poling process. Structural properties along with average crystalline size and lattice strain of PVDF-BTO-rGO nanocomposites were calculated using XRD technique with Williamson-Hall approach. Increment in electroactive β phase from 54 to 73% has been observed by loading rGO in PVDF-BTO nanocomposites. For the first time, optimal rGO content in PVDF-BTO nanocomposites to achieve maximum mechanical properties is studied. Young's modulus, tensile strength, breaking strain, storage modulus, viscosity, and hardness of PVDF-BTO-rGO films showed remarkable increment compared to PVDF-BTO nanocomposites respectively. The PENG devices were subjected to continuous finger tapping, film twisting and thumb pressing using human hand to record piezoelectric output for poled and unpoled samples. The PENG devices displayed significant enhancement in piezoelectric output voltage from 0.98 V for pure PVDF to 4.1 V for PVDF-BTO-rGO when rGO content is 1.25 wt% for finger tapping condition.

Keywords PVDF · Piezoelectricity · Energy harvesting · Nanocomposites · Poling · Nanogenerator

Introduction

The rapid development of polymer nanocomposite based flexible piezoelectric sensors have attracted considerable attention due to their promising applications in nanogenerators [1], structural health monitoring [2], robotics [3], wearable and flexible electronics [4]. Several efforts have been made over the past decade to develop highly flexible piezoelectric devices with a high dielectric constant and good piezo response. A combination of polymers and piezoelectric ceramic materials has been found to be highly effective in fabricating flexible piezoelectric nanocomposites for sensing [5]. Various piezo ceramic materials like PbTiO_3 [6], PMN-PT [7], PZT [8], BaTiO_3 [9–15] etc. have been used to fabricate energy harvesting devices owing to

their excellent dielectric and piezoelectric properties. Due to brittleness and rigidity, ceramics cannot be used for energy harvesting despite their high piezoelectric coefficients. Additionally, they are toxic and highly expensive [16].

Piezoelectric polymers show particular interest in this context due to their low cost, flexible nature, biocompatibility, and ease of fabrication. Amongst all, PVDF is prominently used for energy harvesting because of its higher piezoelectric coefficient and structural flexibility [17]. PVDF has multiple phases like α , γ , β , and δ ; out of which, β phase is of great interest because of its electroactive polar nature. The presence of this phase confers piezoelectric properties that are crucial for energy harvesting applications [18–20].

Different techniques have been tried to enhance energy harvesting performance of ceramic reinforced PVDF nanocomposites. The addition of a carbon based conductive fillers to polymer-ceramic based nanocomposites can improve its piezoelectric performance, allowing the nanogenerator to harvest more energy [21, 22]. The carbon based compound facilitates uniform dispersion of BTO nanoparticles into the

✉ Poonam Kumari
kpmech@iitg.ac.in

¹ Department of Mechanical Engineering, Indian Institute of Technology Guwahati, 781039 Assam, India

polymer solution [23]. Yaqoob et al. reported role of graphene oxide on ferroelectric and dielectric behaviour of PVDF-BTO composites for prospective energy harvester applications. The nanocomposite films were coated on Pt/TiO₂/SiO₂/Si substrate [24]. But, in this work, no poling process is performed, which generally enhances piezo voltage by several orders. Later, Yaqoob et al. reported enhanced output voltage and current values using poling process [25, 26]. Shi et al. studied synergistic behaviour of graphene and BTO nanofillers on energy harvesting performance of PVDF nanofibers. But the harvesting behaviour only up to 0.15wt.% of graphene was reported [9]. Bakar et al. reinforced graphene quantum dots in PVDF-BTO composites to check its energy harvesting capability. A peak to peak voltage of 4.6 V was obtained [27]. Luo et al. fabricated flexible wearable pressure sensor device for electronic skin applications. PVDF-BTO-rGO thin films were fabricated using near-field electro hydrodynamic direct-writing method [28]. Sensing performance only up to 1wt.% rGO was studied. Also, no output voltage was recorded for different rGO concentrations. Li et al. synthesized PVDF-BTO-rGO ternary piezo film with multilayer design having rGO loading up to 0.45 wt%. A maximum voltage of 16.91 V is reported [23].

Very few reports are available on mechanical properties of PVDF-BTO-rGO nanocomposites [29, 30]. Yet, there is no research on the optimal rGO content in PVDF-BTO nanocomposites to achieve maximum tensile strength, toughness, elastic modulus, and hardness. Moreover, the role of rGO loading on viscoelastic behaviour of PVDF-BTO films has not yet been investigated. Reports on the effect of rGO reinforcement on PVDF-BTO nanocomposites' microstructural properties, such as lattice strain and crystal size, are not available yet. Moreover, effect of higher rGO reinforcement (more than 0.45 wt%) on energy harvesting performance of PVDF-BTO composites has not yet been demonstrated. There has not been much research on the energy harvesting behaviour of PVDF-BTO-rGO nanocomposite films made by solvent casting, as most research works have focused on electrospun or spin coated films. In this work, optimal weight fraction of rGO for enhanced mechanical, piezoelectric and thermal behaviour of PVDF-BTO-rGO nanocomposite films fabricated by solvent casting technique is studied. To enhance the β phase content and piezo behaviour, electric poling is performed on the fabricated samples. Additionally, energy harvesting performance is studied for higher loading of rGO in PVDF-BTO nanocomposites.

Experimental

Materials

PVDF pellets (Mw of 530,000), N, N-dimethyl formamide (DMF) (anhydrous, 99.8%) solvent and BTO nanoparticles (< 100 nm size, 99% trace metals basis) were ordered from

Sigma Aldrich, USA. rGO powder (purity > 99%, 3–5 layers) was supplied by Techinstro industries, Nagpur.

Preparation of PVDF-BTO-rGO solution

The nanocomposite films are fabricated using solvent casting process as presented in Fig. 1. Initially, 2 g of PVDF was added to DMF (10 ml) solvent under magnetic stirring for 3 h at 60°C. A 15wt.% BTO was then added to PVDF solution and the resulting mixture is further stirred for another 2 h. Different amount of rGO was added into PVDF-BTO solutions to get 0.5, 0.75, 1, 1.25, and 1.5 wt% of PVDF-BTO-rGO solutions. The prepared solutions were again magnetically stirred at 500 rpm for 4 h before being sonicated for 1 h. Then, the resulting solutions were kept in vacuum desiccator for 30 min. to remove bubbles from the solution. Same procedure is followed for pure PVDF and PVDF-BTO nanocomposite formation. rGO weight fraction was calculated using following relation

$$\text{wt. \% of rGO} = \frac{W_{rGO}}{W_{rGO} + W_{PVDF}} \quad (1)$$

where, W_{rGO} and W_{PVDF} are weights of rGO and PVDF in g respectively. Table 1 provides a detail of each mixture percentages.

Fabrication of PVDF-BTO-rGO films

The degassed solutions were then poured into the petri dish and is kept at 70°C for 12 h in muffle furnace for evaporating the solvent. The free-standing nanocomposite films were obtained once the solvent is removed completely. The resulting films are then compressed between two square-shaped aluminium plates and annealed at 120 °C for approximately 1 h resulting in dense composite with less porosity. The fabricated nanocomposite film is presented in Fig. 2a. The as-prepared nanocomposite films were given the following names for convenience: A (pure PVDF), AB (PVDF-BTO), ABC-0.5, (PVDF-BTO-0.5wt.%rGO), ABC-0.75 (PVDF-BTO-0.75wt.%rGO), ABC-1 (PVDF-BTO-1wt.%rGO), ABC-1.25 (PVDF-BTO-1.25wt.%rGO), ABC-1.5 (PVDF-BTO-1.5wt.%rGO). After the nanocomposite fabrication, the samples were subjected to electric poling process, to further enhance piezoelectric behaviour. At first, Al (aluminium) electrodes (200 nm thick) were thermally evaporated on both sides of nanocomposite films. Al coated films are then placed in between the spring-loaded copper electrode of the poling jig. To prevent any electrical arcing, the test samples were immersed in the silicon oil.

PENG device fabrication

A sandwich structure is cut into 3 cm x 1.5 cm pieces, which are then wrapped in Polyethylene terephthalate (PET) sheets to protect them from damage as shown in Fig. 2b.

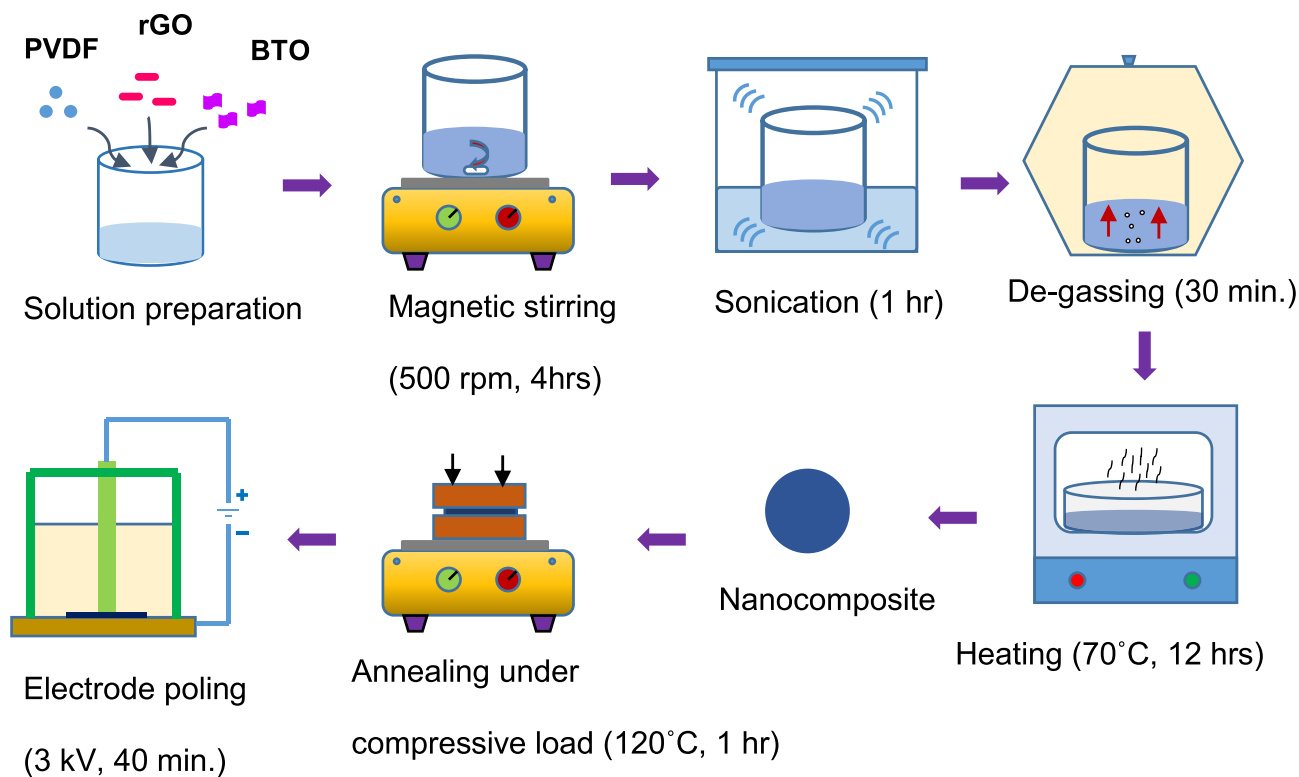


Fig. 1 Step by step process for nanocomposite fabrication using solvent casting approach

Material characterization

FESEM & EDS

The microstructure and surface morphology of solvent cast films were examined with the help of FESEM (GeminiSEM 500, ZEISS) followed by elemental analysis and distribution study using EDS.

Raman analysis

Raman spectra of nanocomposite films were recorded with the help of Laser Micro Raman System (LabRam HR,

Horiba JobinYvon) having 532 nm laser wavelength with 5 s integration time.

FTIR

FTIR (PerkinElmer, Singapore) of the nanocomposite films were performed over the wavenumber range of 400–3500 cm^{-1} in ATR mode.

XRD

Phase and crystal plane analysis was performed using XRD (Rigaku, Japan) having $\text{Cu K}\alpha$ radiation with 1.54 Å wavelength over the 2θ span from 15–80° with a scan rate of 4°/min.

Table 1 Amount of matrix and fillers for nanocomposite fabrication

Sample	Weight of PVDF (g)	Weight of BTO (g)	Weight of rGO (g)	Volume fraction of rGO (%)
A	2	-	-	-
AB	2	0.36	-	-
ABC-0.5	2	0.36	0.01	6.5
ABC-0.75	2	0.36	0.015	9.4
ABC-1	2	0.36	0.02	12.2
ABC-1.25	2	0.36	0.025	14.8
ABC-1.5	2	0.36	0.03	17.3

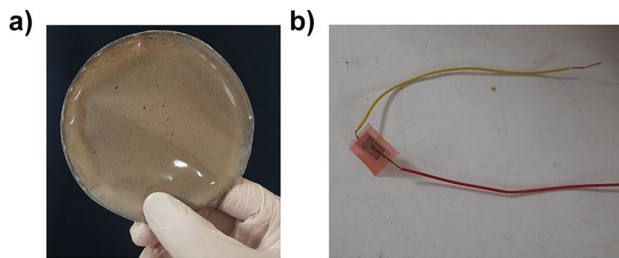


Fig. 2 a Solvent casted nanocomposite film, b fabricated PENG device

TGA

Thermal stability and mass loss of nanocomposite films was analysed from 20°C–800°C at 10°C/min using TGA instrument (TGA 4000, PerkinElmer).

DSC

Nanocomposite films were heated from 25°C–250°C at 10°C/min for DSC test (STA449F3A00, Netzsch) under Argon gas atmosphere.

UTM testing

Mechanical properties (elastic modulus, tensile strength, and toughness) of the nanocomposite films were determined with an Instron dynamic UTM 8801 (100 kN) machine at a velocity of 1 mm/min. To prepare the samples for the tests, ASTM standard D882 was followed.

Rheometer

The viscosity was measured using (Physica MCR 301, Anton Paar) rheometer at room temperature with a fixed strain of 1%.

DMA

The viscoelastic behaviour of the nanocomposite films was studied using a DMA (Physica MCR 702, Anton Paar) in tensile mode on a 40 × 10 mm sample size. The films were subjected to a frequency sweep from 0.1 to 100 Hz at room temperature condition.

Hardness

The hardness values of the nanocomposite samples were determined using Vickers micro hardness test using micro hardness tester (Omni tech, MVH-II). Each sample is subjected to a load of 0.2 kgf for 20 s.

Dielectric measurement

The dielectric property measurement was performed using LCR meter (Hioki, IM 3536) from 4 Hz to 8 MHz at room temperature. The test samples were cut into rectangular shapes of about 3 mm × 3 mm, and aluminium (Al) electrode coating (about 200 nm thick) was applied on both sides.

Output voltage measurement

The piezo response of fabricated piezoelectric nanogenerators (PENGs) was recorded using digital oscilloscope (GWInSTEK, GDS-2102 A).

Results and discussion

FESEM & EDS

FESEM plots of rGO and BTO nanoparticles are shown in Fig. 3a, b respectively. BTO displays a spherical structure whereas rGO shows a sheet-like structure. The diameter distribution spectra presented in Fig. 3c show that BTO nanoparticles have an average particle size of 75.86 ± 20 nm. Figure 3d, e shows grain structure of pure PVDF and BTO loaded PVDF matrix respectively. rGO and BTO particles are completely dispersed and well covered in PVDF, confirming successful fabrication of PVDF-BTO-rGO nanocomposites, as presented in Fig. 3f, g. Dense rGO sheets with embedded BTO particles at certain locations can be found in Fig. 3f. EDS spectra in Fig. 4a–d indicate fluorine (F), oxygen (O), carbon (C), titanium (Ti), and barium (Ba) elements are mainly present in the sample, which confirms the successful fabrication of PVDF-BTO-rGO nanocomposite films. The energy levels of F, Ba, Ti, O, and C elements in the polymer matrix are 0.5 keV, 4.46 keV, 4.5 keV, 0.6 keV, and 0.24 keV, respectively [31, 32]. Elemental mapping as shown in Fig. 4e, f confirms uniform distribution of the constituent elements inside PVDF matrix.

Raman spectroscopy

Figure 5a, b shows Raman spectra for pure rGO and rGO loaded polymer composites. Raman spectroscopy is helpful in characterization of material structure and defects in rGO based materials. The intense peak at 308 cm^{-1} and small peak at 720 cm^{-1} corresponds to tetragonal crystal structure of BTO [33]. The peaks at 1431 and 2974 cm^{-1} belongs to PVDF matrix [34]. A D peak at 1326 cm^{-1} and a G peak at 1573 cm^{-1} were observed for rGO which specifies defects and sp^2 carbon networks of the samples under test. The intense peak at 2974 cm^{-1} and weak peak at 1431 cm^{-1} represents C–H and $-\text{CH}_2$ bond vibrations respectively. The D and G peaks of ABC 0.5 were not as intense due to the lower filler content of rGO. ABC 1 showed maximum intensity for D band, thereby signalling more defects on rGO sheets. The intensity ratio values shown by different nanocomposite samples are presented in Table 2.

FTIR spectroscopy

The FTIR plot shown in Fig. 5c is utilised to explore PVDF's crystalline forms in more detail. The vibrational bands at 763 cm^{-1} and 976 cm^{-1} are associated with the non-polar α phase [35], while the characteristic peaks at 841 cm^{-1} and 1231 cm^{-1} are associated with the electroactive β phase [36, 37]. Symmetric tensile vibrations of $-\text{CF}_2$ and C–C produce

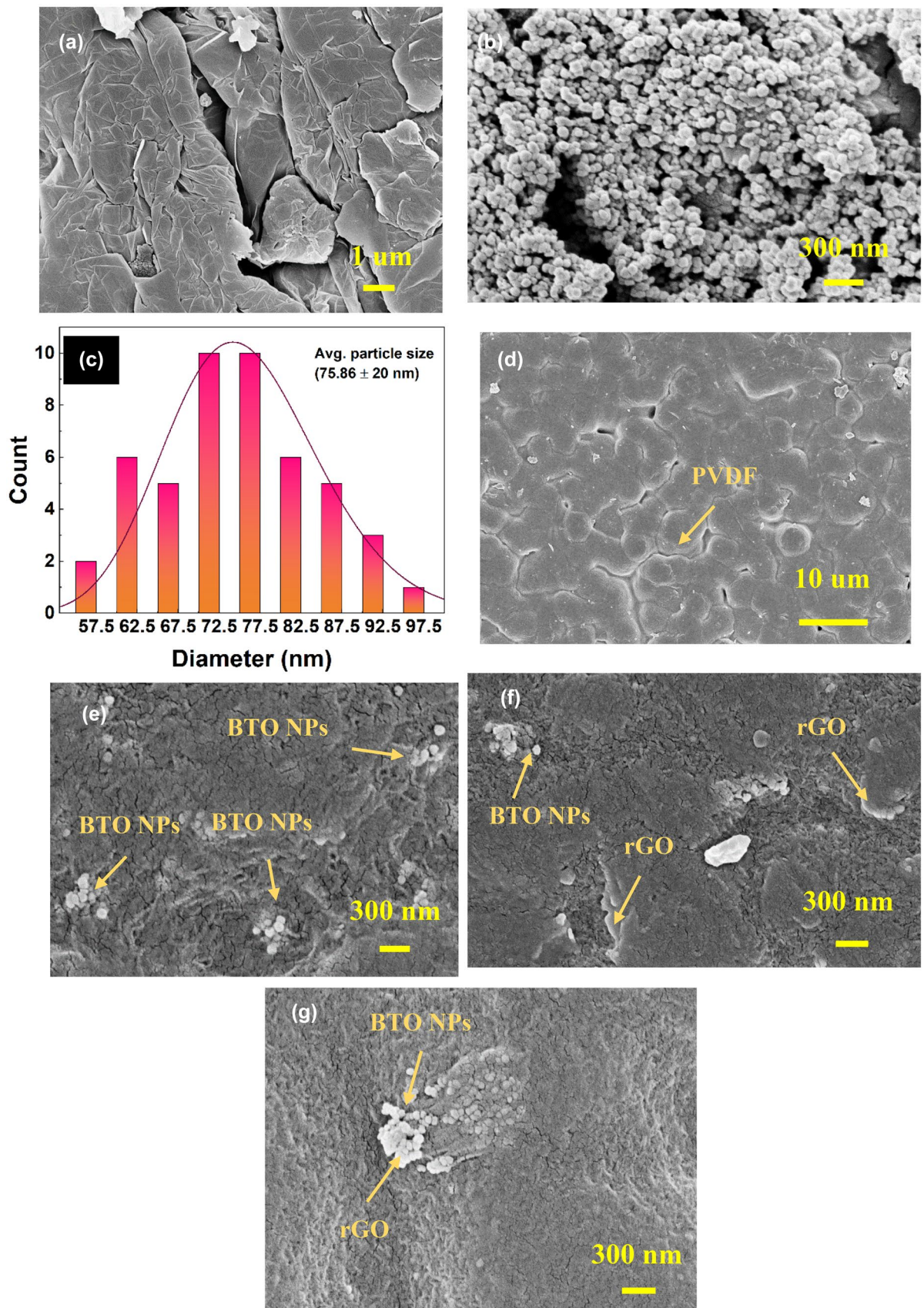


Fig. 3 FESEM images of **a** rGO nanosheets, **b** BTO nanoparticles, **c** BTO nanoparticle size distribution, and samples **d** A, **e** AB, **f** ABC 0.75, and **g** ABC 1.5

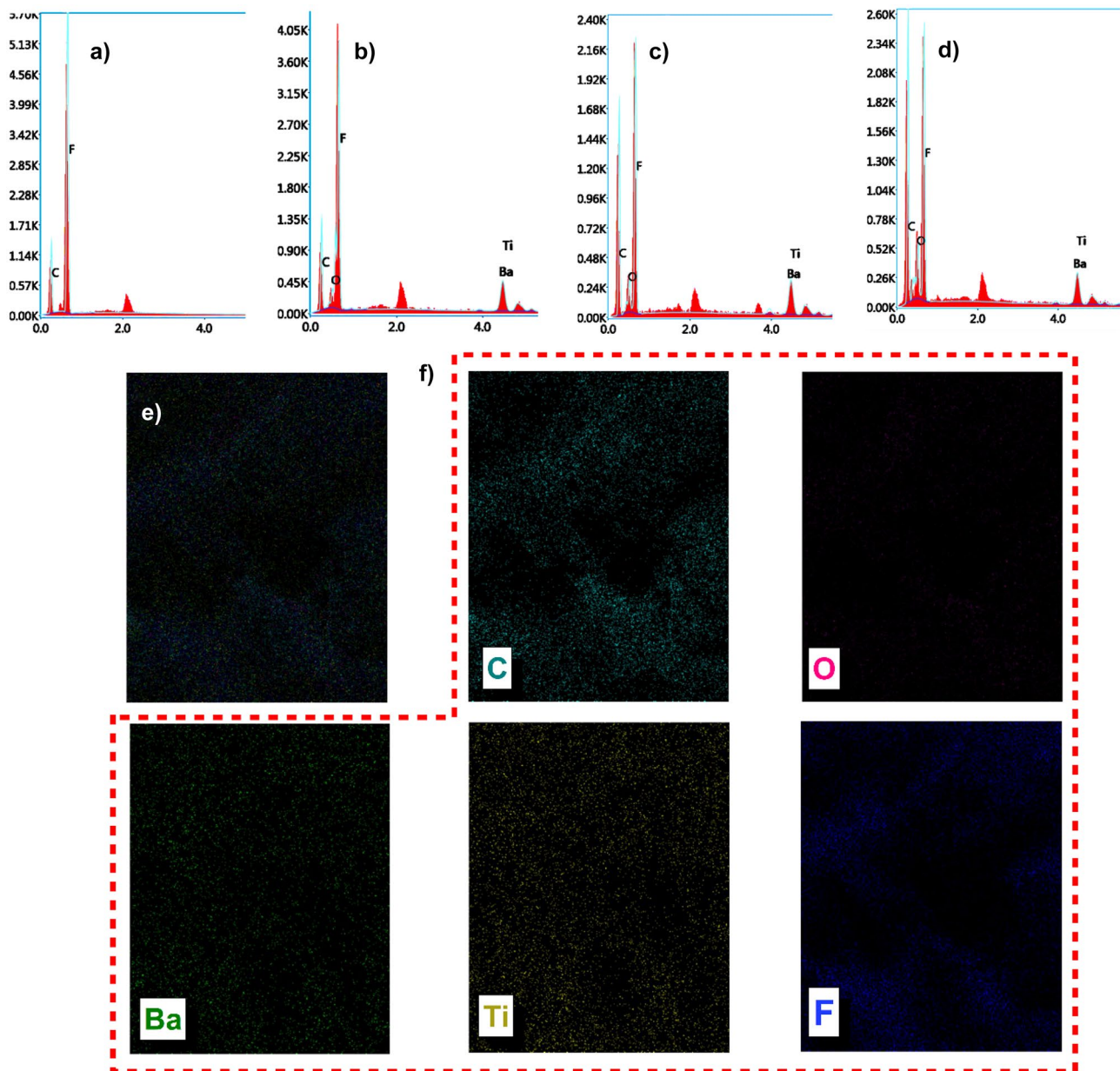


Fig. 4 EDS spectra for sample **a** A, **b** AB, **c** ABC 0.75, and **d** ABC 1.5. **e** all the mapping elements. **f** mapping image of each constituent element for ABC 0.75

the absorption peaks at 842 and 1288 cm^{-1} , whereas $-\text{CH}_2$ swing antisymmetric stretching of C–C produces the absorption peak at 1400 cm^{-1} [38]. The fraction of β phase in solvent casted films is calculated by Gregorio formulae [39]

$$F(\beta) = \frac{A_{841}}{\left(\frac{K_{841}}{K_{763}}\right)A_{763} + A_{841}} = \frac{A_{841}}{1.26 * A_{763} + A_{841}} \quad (2)$$

where A_{841} and A_{768} are absorbance values at 841 cm^{-1} and 763 cm^{-1} whereas K_{841} and K_{768} are coefficients of absorption for the corresponding wavenumber values, which corresponds

to 6.1×10^4 and $7.7 \times 10^4\text{ cm}^2 \cdot \text{mol}^{-1}$, respectively. It can be observed that, β phase content in nanocomposite films, especially in rGO reinforced films, are higher than neat PVDF

Table 2 Intensity ratio values for different nanocomposite samples

Sample	Intensity ratio
ABC 0.5	0.36
ABC 0.75	0.23
ABC 1	0.94
ABC 1.25	0.65
ABC 1.5	0.93

films. As rGO loading increases, the increment in β phase content continues until the loading reaches 1.25 wt%, followed by a drastic reduction. β phase content of 54, 58, 66, 69, 73, and 70% was obtained corresponding to samples with rGO reinforcement of 0, 0.5, 0.75, 1, 1.25, and 1.5 wt% respectively as presented in Fig. 5d. The significantly enhanced β phase content results from the improved interaction between local electric field surrounding the nanofiller and PVDF dipoles, where the rGO sheets act as nucleating agents to facilitate β phase formation [9, 40]. The reduction in β phase content value may be attributed to agglomeration of rGO sheets causing hindrance to PVDF molecular chains motion.

XRD measurement

The effect of rGO loading on phases and structure of nanocomposite films is investigated using XRD analysis. Diffraction peaks of rGO and BTO powder are presented in Fig. 6a, b. A diffraction peak at 20.36° represents electroactive β phase of PVDF occurred due to diffraction of (200) and (110) crystal planes [41]. The peaks shown at $2\theta = 22.07^\circ, 31.53^\circ, 38.89^\circ, 45.23^\circ, 50.98^\circ, 56.17^\circ, 65.89^\circ, 70.46^\circ, 74.88^\circ,$ and 79.16° belong to miller planes of (100), (110), (111), (200), (210), (211), (320), (300), (310), and (311) respectively. The peak at $2\theta = 26.51^\circ$ corresponds to rGO. The interaction between PVDF and rGO has a direct effect on β phase content of PVDF. On rGO addition, $-\text{CF}_2$ dipole of PVDF

matrix and $-\text{CH}_2$ dipole of rGO orientate with each other which causes enhancement of polar β phase of PVDF matrix [42]. The XRD plots of PVDF-BTO-rGO nanocomposites are shown in Fig. 6c, d. nanocomposite Further, Williamson-Hall (W-H) method with uniform deformation model (UDM) is applied to calculate the average crystalline size and lattice strain induced in the sample. UDM only considers isotropic strain, which generally affects the physical broadening of the XRD profile. The equation used to calculate the crystal parameters is given as

$$\delta_{hkl} \times \cos \theta = \frac{0.9\lambda}{D} + 4\mu \sin \theta \quad (3)$$

where δ_{hkl} is Full width at half of the maximum intensity (FWHM) for different planes, D is average crystalline size, μ is lattice strain, and λ is the wavelength. Crystalline size and strain values were calculated by plotting $(4\sin\theta)$ along X-axis and $(\delta_{hkl} \cdot \cos\theta)$ along Y-axis, followed by straight-line fit ($R^2 = 0.8954$). The slope represents lattice strain in this straight line, while the intercept represents crystal size. Average crystalline size of BTO nanoparticles is found to be 65 nm, as shown in Fig. 6e. Calculated structural parameters are given in Table 3.

TGA

Role of presence of nanofillers on thermal stability of PVDF matrix was analysed using TGA study as shown in Fig. 7a.

Fig. 5 Raman plot of **a** pure rGO and **b** PVDF-BTO-rGO nanocomposite films for different rGO content, **c** FTIR spectra and **d** fraction of electroactive β phase content against varying rGO content for PVDF-BTO-rGO nanocomposite films

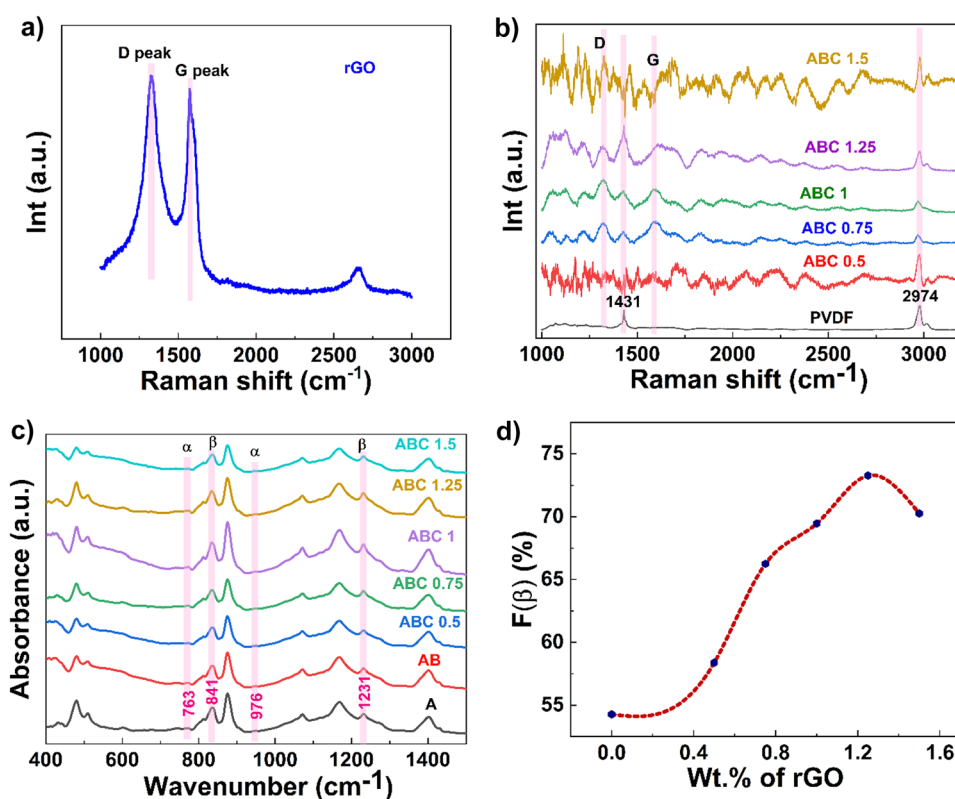
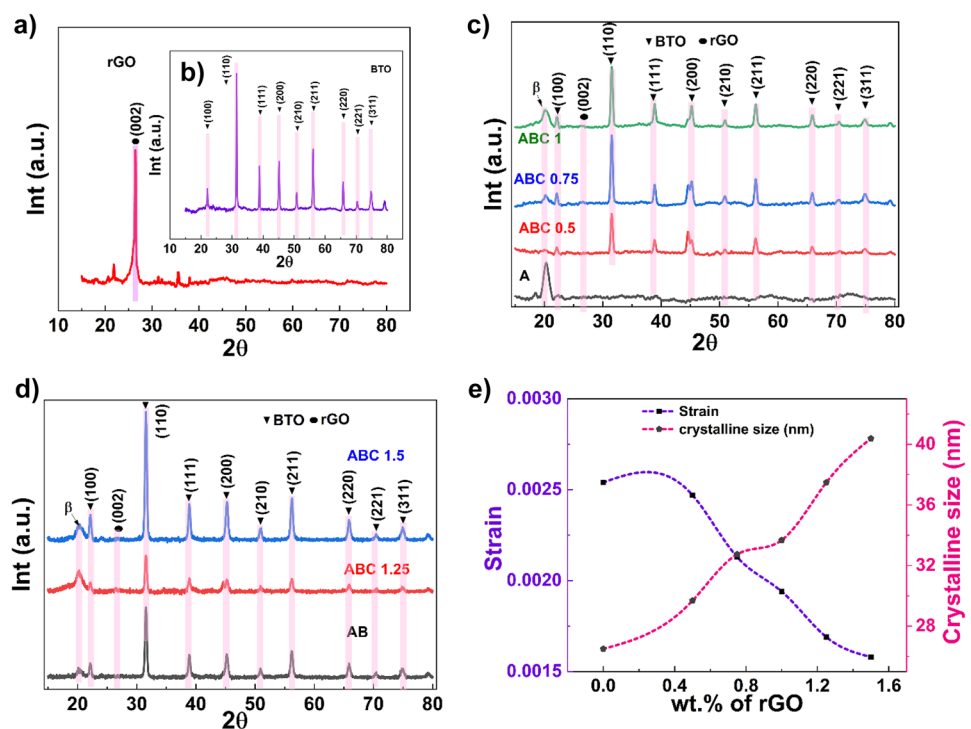


Fig. 6 XRD patterns of **a** rGO nanosheets, **b** BTO nanoparticles, **c** A, ABC 0.5, ABC 0.75, ABC 1, and **d** AB, ABC 1.25 and ABC 1.5 nanocomposite films, **e** crystalline size and induced strain



For pure PVDF, sudden thermal decomposition at around 425°C is observed leading to weight loss of about 60% at around 490°C followed by more gradual thermal degradation. Incorporation of BTO nanoparticles (20 wt%) in PVDF matrix show significant enhancement in thermal stability. BTO nanoparticles and the PVDF matrix have a large surface area of contact, which restricts the thermal breakdown of the PVDF chain. In addition, PVDF-BTO nanocomposites were reinforced with secondary rGO nanofillers to test their thermal stability. A further increase in thermal stability was observed as rGO content was increased. The enhanced thermal stability is attributed to the barrier effect of rGO, which restricts thermodegradation [43]. As a result of their synergistic effect, BTO and rGO reduce thermal degradation rate, thereby improving the thermal performance of PVDF-BTO-rGO nanocomposite. Additionally, better dispersion of nanofillers into the PVDF matrix can increase the activation energy for thermal degradation. Increment in onset

temperature (T_{onset}) has been observed on reinforcing BTO particles whereas in nanocomposites added with rGO, T_{onset} values enhance significantly. Sample ABC 1.5 showed maximum T_{onset} of 480.47°C, an increase of 44°C compared to PVDF. Increased percentage of residual mass (m_r) on nanofiller addition also confirms the enhanced thermal stability of nanocomposite samples. Sample ABC 1.5 showed a maximum residual mass of 32.25% at 750°C. T_{onset} and m_r values of all the tested samples are presented in Table 4. The obtained results suggest that the flexible nanocomposite films can be implemented in the thermally stable domain for the prospective nanogenerator applications.

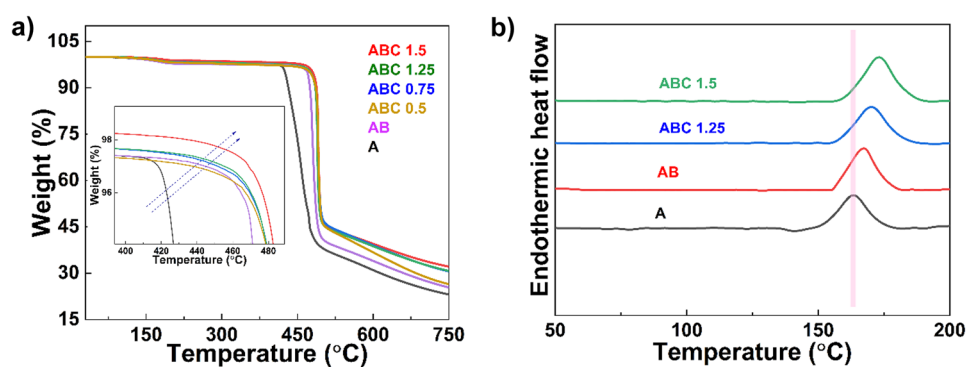
Table 3 XRD structural parameters for nanocomposites

Sample	Crystalline size (nm)	Lattice strain
AB	26.5	0.00254
ABC 0.5	29.68	0.00247
ABC 0.75	32.74	0.00213
ABC 1	33.67	0.00194
ABC 1.25	37.48	0.00169
ABC 1.5	40.38	0.00158

DSC measurement

The role of rGO nanofillers on thermal behaviour of PVDF-BTO nanocomposites was analysed using DSC plots as presented in Fig. 7b. The analysis comprised four samples (A, AB, ABC 1.25 and ABC 1.5). Gradual increment in melting temperature was observed with increasing rGO content in PVDF-BTO nanocomposites. The large surface area of rGO sheets makes them ideal nucleating agents because of their ability to adsorb PVDF chains and cause nucleation as a result [43]. Degree of crystallinity (X_c) of nanocomposite samples were calculated using following relation

$$X_c = \frac{\Delta H_{mt}}{\Delta H_{100\%}} \times 100 \quad (4)$$

Fig. 7 a TGA and b DSC plots for nanocomposite samples

where, ΔH_{mt} is enthalpy associated with melting, $\Delta H_{100\%}$ is enthalpy associated with 100% crystalline PVDF (104.7 J/g) [44]. BTO reinforcement increases the crystallinity of PVDF matrix. The crystallinity values of PVDF-BTO nanocomposites are further enhanced by adding rGO as a secondary nanofiller. Increasing crystallinity is caused by changes in filler reinforcement, nanofiller size, and interfacial interactions of nanofillers with PVDF matrix [45, 46]. Values of ΔH_{mt} , and X_c for nanocomposite samples are listed in Table 4.

UTM testing

It is essential that an excellent piezoelectric material possess good mechanical properties if it is to be used in energy harvesting, self-powering device applications. Effect of rGO loading on mechanical properties of PVDF-BTO nanocomposites were studied in tensile measurements as shown in Fig. 8a–c. It was observed that, on increasing the rGO concentration up to certain extent, tensile strength and elastic modulus is also increased. A drastic reduction in strength and elastic modulus was observed for 1.5 wt% of rGO loading. Apparently, this is caused by agglomeration of rGO sheets in a PVDF-BTO heterogeneous system. A maximum tensile strength and elastic modulus of 41.43 MPa and 1215.2 MPa was observed for ABC 1.25 sample. Reduction in the breaking strain was observed for higher concentrations of rGO, confirming ductile to brittle transformation of nanocomposite films. The poor dispersion of rGO and BTO fillers lead to micro-nanoscale voids and defects causing stress

concentration at different locations in the PVDF matrix. This leads to enhanced brittleness and reduction in breaking stress and strain values [47]. Maximum breaking strain of 0.36 was observed for sample A. For all samples, toughness values were calculated by following the area under stress-strain curve up to breaking point. The toughness value increased for sample AB, and then decreased for samples with rGO content. Sample AB showed maximum toughness value (6.08 ± 0.2). A summary of mechanical properties is presented in Table 5. Values of toughness, breaking strain and max. tensile strength obtained are considerably higher than previously reported result [48].

Viscosity measurement

The rheological behaviour of nanocomposite solutions was studied for sample A, AB and ABC 1.25 respectively. Variation of viscosity with frequency is presented in Fig. 9. The viscosity of all tested solutions decreased with increasing frequency. The viscosity increases with increasing nanofiller content, and the rGO effect is most pronounced at low frequencies. Among the tested solutions, sample A possessed the lowest viscosity, while sample ABC 1.25 possessed the highest. Sample ABC 1.25 showed steepest viscosity curve among the tested samples for lower frequency values. It is confirmed with viscosity measurements that on BTO and rGO addition, solid like effective networks are formed, thereby blocking PVDF chain movement and increasing interfacial bonding between these chains and nanofillers [49].

Table 4 TGA and DSC parameters for PVDF nanocomposites

Sample	T_{onset} (°C)	m_r (%)	ΔH_{mt} (J/g)	X_c (%)	T_m (°C)
A	430.19	23.14	24.23	23.15	163.4
AB	469.58	25.37	25.2	24.06	167.37
ABC 0.5	474.5	26.47	-	-	-
ABC 0.75	475.65	30.59	-	-	-
ABC 1.25	475.75	30.73	25.89	24.72	170.24
ABC 1.5	480.47	32.25	30.09	28.73	173.23

DMA analysis

The dynamic mechanical analysis can be used to explore interactions between nanoparticles and polymer matrix in nanocomposites [50]. Mechanical properties like storage and loss moduli over desired frequency ranges are evaluated using this test. Figure 10a shows rectangular nanocomposite films for DMA measurement, whereas Fig. 10b presents state of the sample (as shown by dotted red lines)

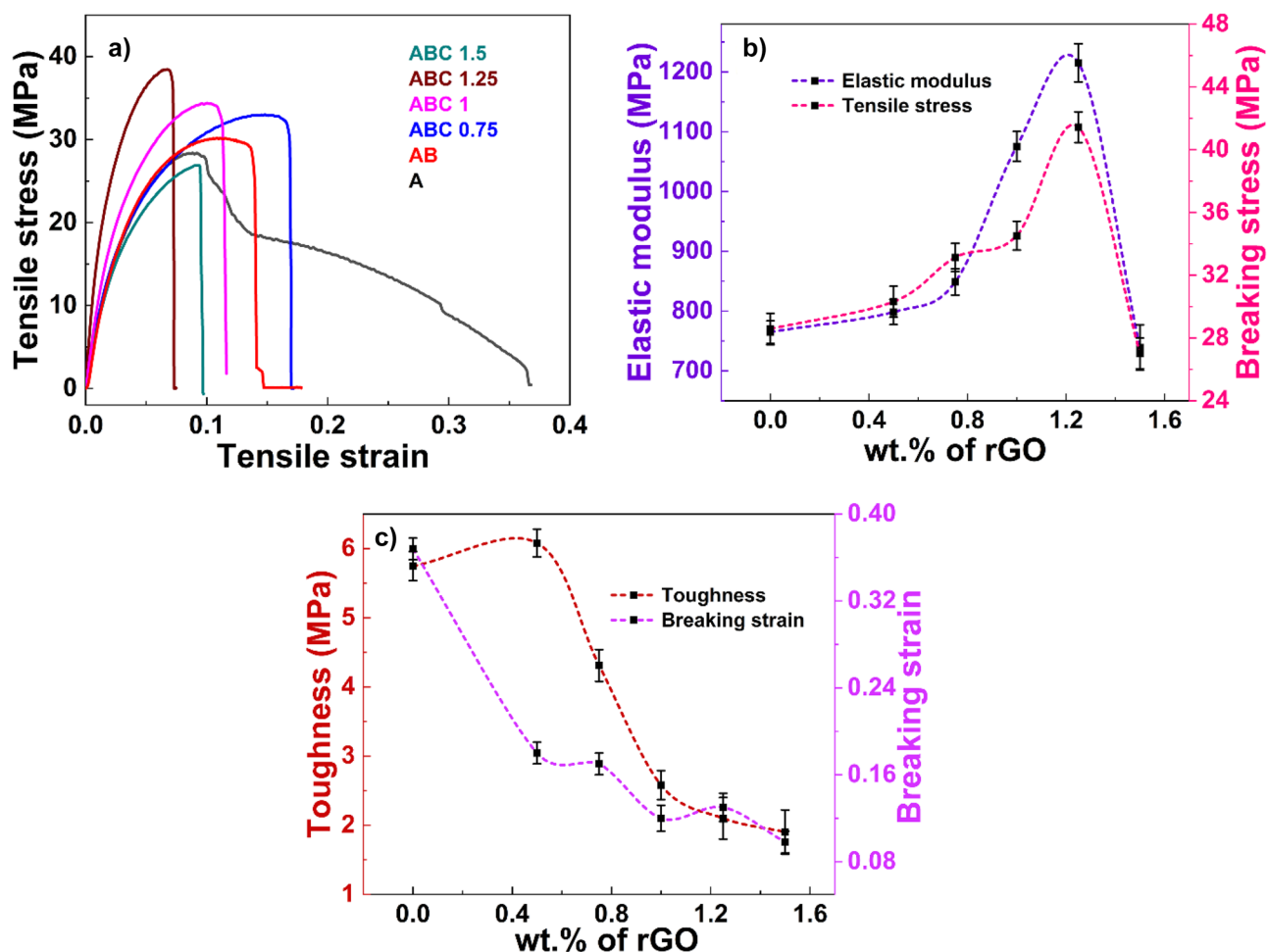


Fig. 8 a Stress-strain plot, role of rGO concentration on b elastic modulus, c tensile stress, d breaking strain and e toughness of PVDF-BTO-rGO nanocomposite films

under prospective loading condition for dynamic response measurement. The plot of storage modulus vs. frequency as shown in Fig. 10c demonstrates the effect of nanofillers on storage modulus values. Nanocomposites are better at distributing interfacial stress and limiting the segmental motion of polymer matrix chains than pure PVDF [51]. It is observed that, all the nanocomposite samples displayed enhanced storage modulus values compared to pure PVDF.

The high elastic modulus and high strength of rGO and BTO nanofillers are responsible for the enhancement of storage modulus. This increment in storage modulus is attributed to reinforcing effect of nanofillers in PVDF matrix. Sample ABC 1.25 showed a maximum storage modulus value, whereas sample ABC 1.5 showed drastic reduction as compared to other nanocomposites in storage modulus. The agglomerates formed by the accumulation of heavily

Table 5 Mechanical properties of nanocomposites

Sample	Max. tensile stress (MPa)	Breaking strain	Elastic modulus (MPa)	Toughness (MPa)
A	28.57 ± 1	0.36 ± 0.01	764.82 ± 19	5.74 ± 0.21
AB	30.31 ± 0.99	0.18 ± 0.01	798.36 ± 21	6.08 ± 0.2
ABC 0.75	33.13 ± 0.91	0.17 ± 0.01	848.73 ± 22	4.31 ± 0.23
ABC 1	34.52 ± 0.92	0.12 ± 0.012	1075.4 ± 25	2.58 ± 0.21
ABC 1.25	41.43 ± 0.98	0.13 ± 0.013	1215.2 ± 32	2.1 ± 0.3
ABC 1.5	27.02 ± 0.98	0.09 ± 0.01	739.08 ± 38	1.9 ± 0.32

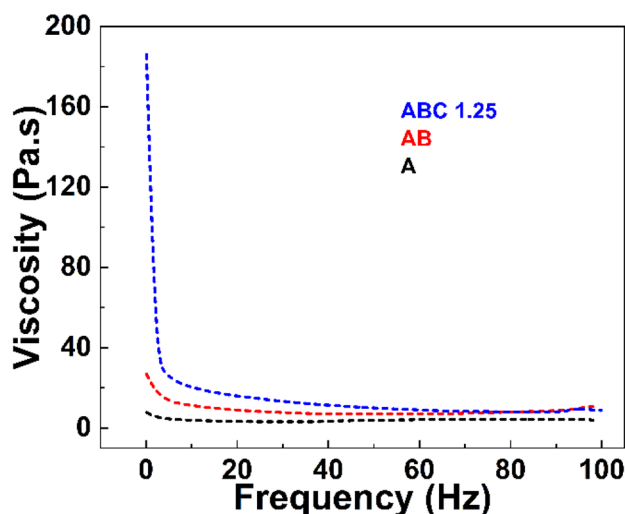


Fig. 9 Variation of viscosity of different nanocomposite solutions with frequency

reinforced nanofillers may be responsible for this reduction. The behaviour of damping factor ($\tan \delta$) against frequency values is shown in Fig. 10d. A slight increment in $\tan \delta$ values is observed for nanocomposites with increasing nanofiller content. The increase is ascribed to the nanocomposites' less elastic nature as a result of the development of multiple filler networks inside the composites [52]. As a result, rGO optimized storage modulus values for PVDF-BTO nanocomposites up to 1 wt% reinforcement, leading to drastic reductions at higher loadings.

Hardness measurement

The nature of polymer-nanofiller interface determines the micro hardness of nanocomposite samples. Surface indentation plots and micro-hardness values of the nanocomposite samples are presented in Fig. 11. Points 1, 2, 3, 4, 5, 6 and 7 in Fig. 11b corresponds to samples A, AB, ABC 0.5, ABC 0.75, ABC 1, ABC 1.25, and ABC 1.5 respectively. BTO addition in PVDF matrix enhances the overall hardness value of PVDF-BTO nanocomposite. The reason behind this increment in micro hardness value is may be due to better interfacial adhesion between polymer and nanofiller. On rGO addition, micro hardness value increased further up to 1.25 wt% of rGO loading, then reduced. The hardness values obtained are 16 ± 1.54 , 24.13 ± 1.14 , 28.57 ± 1.12 , 33.82 ± 1.45 , 41.42 ± 1.98 , 48.18 ± 2.45 , and 38.26 ± 2.6 for A, AB, ABC 0.5, ABC 0.75, ABC 1, ABC 1.25, and ABC 1.5 respectively. rGO nanosheets are among the hardest materials on earth. As a result, it improved the polymer's hardness when it was incorporated into a PVDF matrix [53].

Additionally, rGO sheets have been found to improve the hardness of polymers in various other studies [53, 54]. This is because of the hard phase of rGO sheets present in the PVDF matrix. The rGO interlocks the molecular chains of PVDF, thereby constraining the chain mobility when load is applied [55]. But, at higher rGO loading, this interaction starts degrading due to agglomeration of nanofillers in the PVDF matrix, resulting in reduction in micro-hardness value. As mentioned in tensile test measurements, agglomeration occurs at higher filler loading, which have adverse impact on the hardness values.

Dielectric measurements

The variation in dielectric behaviour of PVDF-rGO-BTO nanocomposites over the frequency range was studied as shown in Fig. 12a. Dielectric properties of PVDF-BTO nanocomposites are significantly affected by rGO loading. The dielectric constant increases as the rGO content increases. A sample ABC 1.5 showed a maximum dielectric constant of 61 at 1 kHz, gradually decreasing to 37 at 8 MHz. At lower frequencies, high dielectric values are caused by the Maxwell-Wagner-Sillars (MWS) theory of interfacial polarization at the insulator-conductor interface [40]. However, at higher frequencies, electric dipoles do not get enough time for its alignment because of rapidly increased electric field causing reduction in dielectric values [56]. Lower dielectric loss was observed at lower frequencies, followed by an increment at higher frequencies. The behaviour of ac conductivity of nanocomposites is presented in Fig. 12b. rGO being highly conductive, improves the overall conductivity of nanocomposite samples upon its addition. Sample ABC 1.5 showed maximum ac conductivity of $4.18 \mu\text{S/m}$ at 1 kHz.

Piezoelectric measurement

Before fabricating the PENG devices, the respective samples were subjected to electric poling using DC poling unit ($50 \text{ kV} @ 5 \text{ mA}$, Ujwal Electronics) as shown in Fig. 13. A voltage of 3 kV is used for about 40 min to align ferroelectric dipoles of BTO and PVDF. A total of seven PENG devices were fabricated and tested under soft tapping, twisting and thumb pressing conditions as presented in Fig. 14. On testing, it is observed that output voltage shown by nanocomposite films is significantly enhanced due to nanofiller addition. Initially, on BTO addition, increment in piezo voltage was observed. But, on addition of secondary nanofiller rGO, piezo voltage and current is enhanced further with increasing rGO loading. rGO facilitates dipole alignment of PVDF matrix and allows micro-capacitor

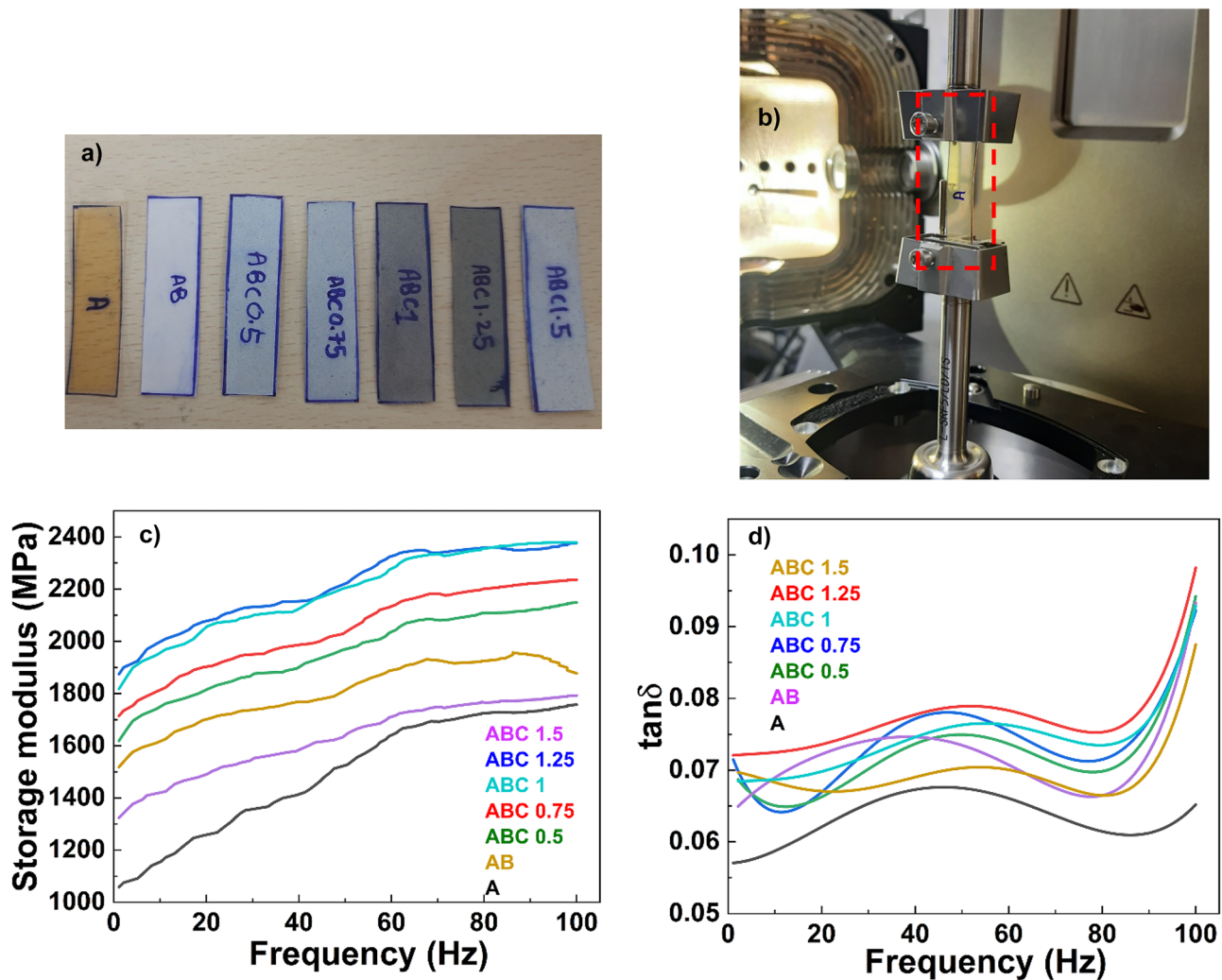


Fig. 10 **a** Samples to be analysed for DMA, **b** sample loading position under dynamic loading condition, DMA results of variation of **c** storage modulus, and **d** damping factor over specified frequency range

model formation inside the nanocomposite. Carbonyl and carboxyl groups in the rGO basal plane play an important role in aligning polymer chains by attracting fluorine atoms. rGO sheets have a large number of free charges on their surfaces as a result of their high mobility. Dipoles generated by PVDF and BTO fillers accumulate these free charges in ceramic-polymer composites, generating new dipoles there. Consequently, the sheet will generate and store more charge as a result of the increased number of dipoles. In conclusion, RGO nanofiller enhances the energy harvesting capacity of PENG device [24]. It is noticed that, a maximum o/p voltage of 4.1 V is obtained for finger tapping condition for rGO concentration of 1.25 wt%. Finger tapping and twisting yielded substantially greater output voltage for increased rGO loading compared to thumb

pressing conditions. The enhanced output signals are attributed to increment in β phase of PVDF, as confirmed in FTIR results. Poling process maximize electric dipole alignment of β phase. However, this increment is stopped for ABC 1.5 showing reduction in piezo response. An overview of piezo voltage behaviour for nanocomposites under different loading conditions with respect to changing rGO loading is presented in Fig. 15a. To confirm the effectiveness of electrode poling operation, piezo responses of poled and unpoled samples of a same concentration are compared under soft tapping, twisting and thumb pressing conditions as shown in Table 6. A significant increment in output voltage is observed for all the nanocomposite samples after electrode poling process under different loading conditions as presented in Fig. 15b–d.

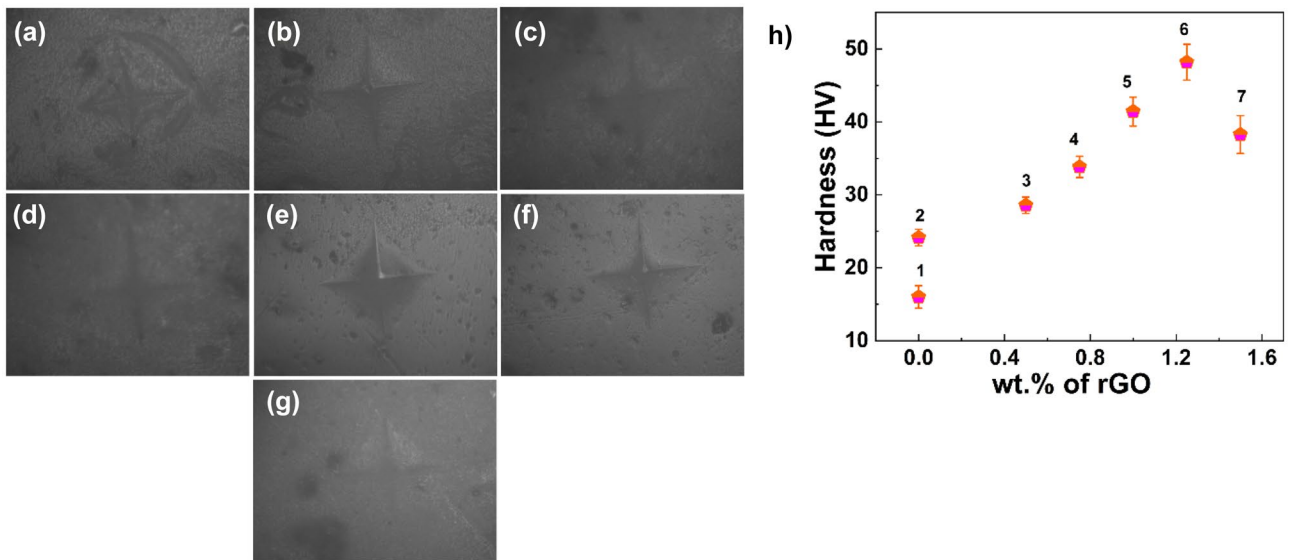


Fig. 11 Surface image after micro indentation for **a** A, **b** AB, **c** ABC 0.5, **d** ABC 0.75, **e** ABC 1, **f** ABC 1.25, and **g** ABC 1.5, **h** micro-hardness values for nanocomposite samples

Fig. 12 Variation of **a** dielectric constant, and **b** ac conductivity for pure PVDF and nanocomposite samples

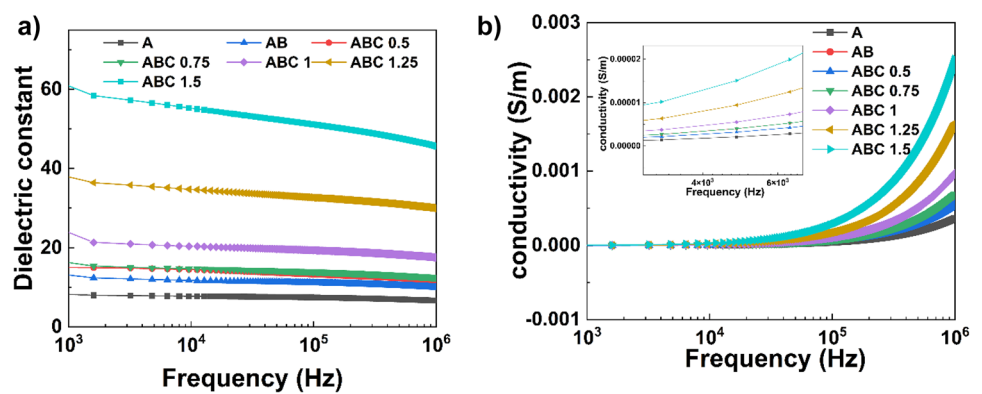
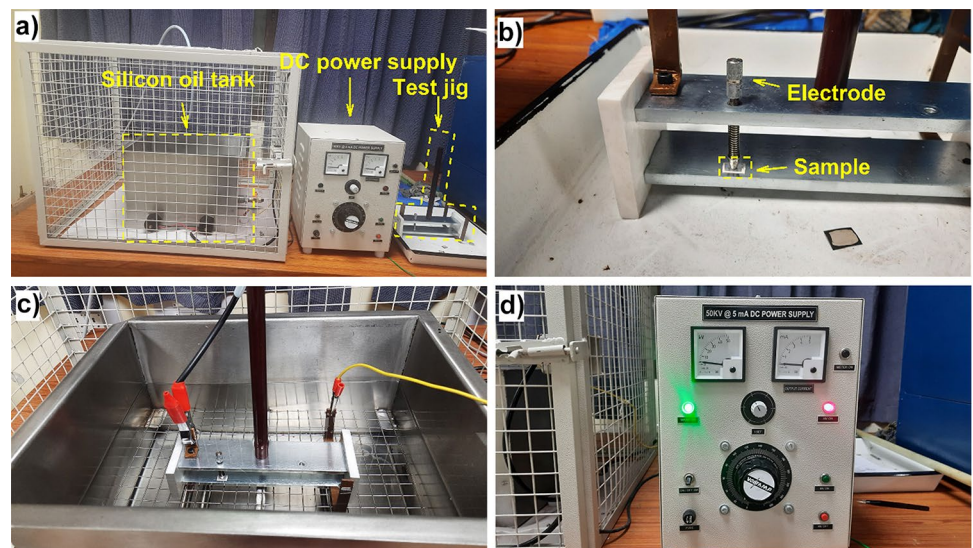


Fig. 13 **a** Electrode poling setup, **b** sample under loading condition, **c** electrical connections before poling, **d** ongoing poling operation



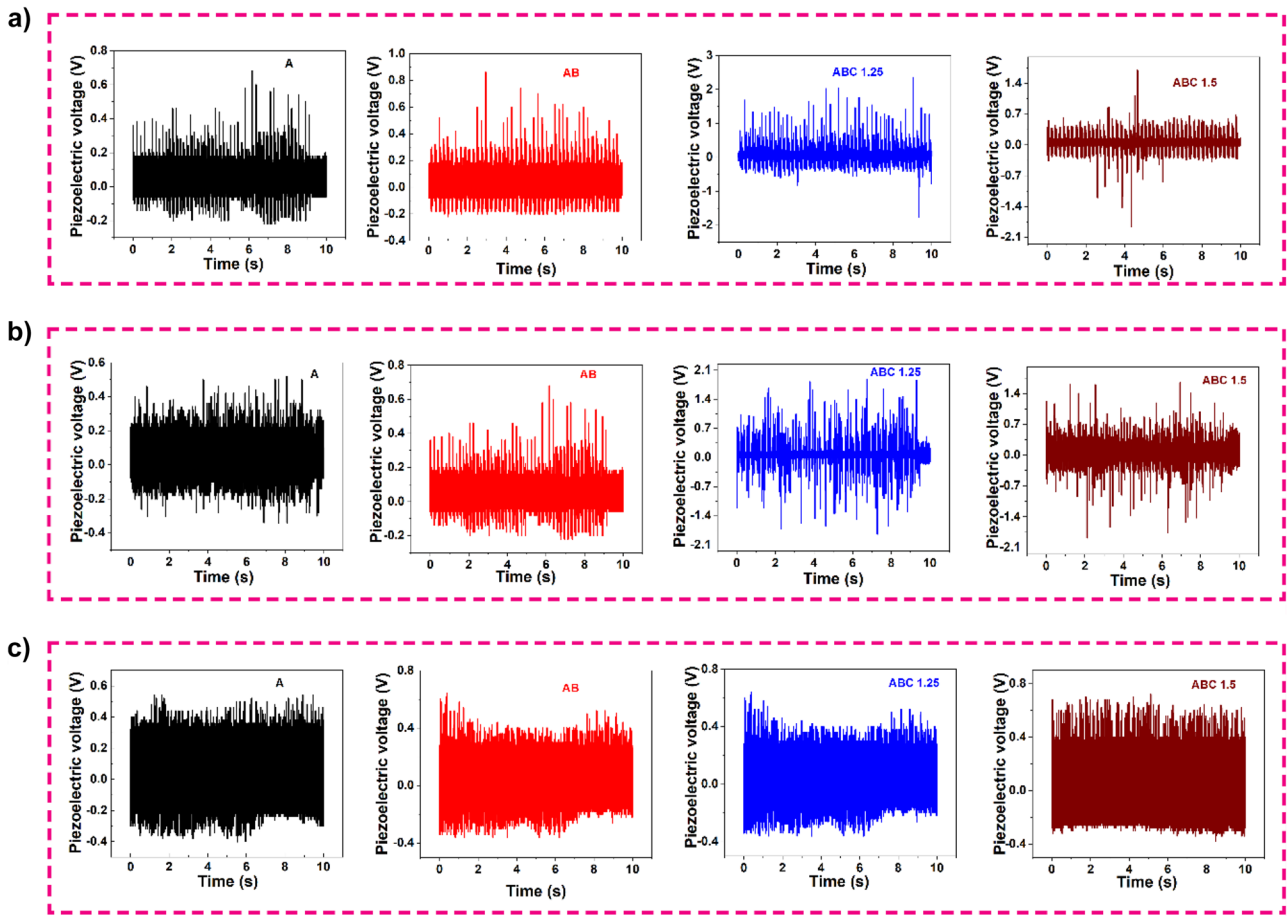


Fig. 14 Piezo voltage of A, AB, ABC 1.25 and ABC 1.5 for **a** finger tapping, **b** twisting and **c** thumb pressing conditions, after electrode poling

Table 6 Voltage measured on test samples for different loading conditions

Sample	Finger tapping (V)		Twisting (V)		Thumb pressing (V)	
	with poling	w/o poling	with poling	w/o poling	with poling	w/o poling
A	0.98	0.3	0.86	0.4	0.94	0.25
AB	1.08	0.38	0.98	0.32	1	0.41
ABC 0.5	1.64	0.42	1.1	0.41	0.98	0.2
ABC 0.75	2.18	0.5	1.08	0.47	1.16	0.47
ABC 1	3.14	0.57	1.15	0.58	1.32	0.38
ABC 1.25	4.1	0.62	3.72	0.73	1.44	0.73
ABC 1.5	3.56	0.64	3.6	0.29	1.12	0.64

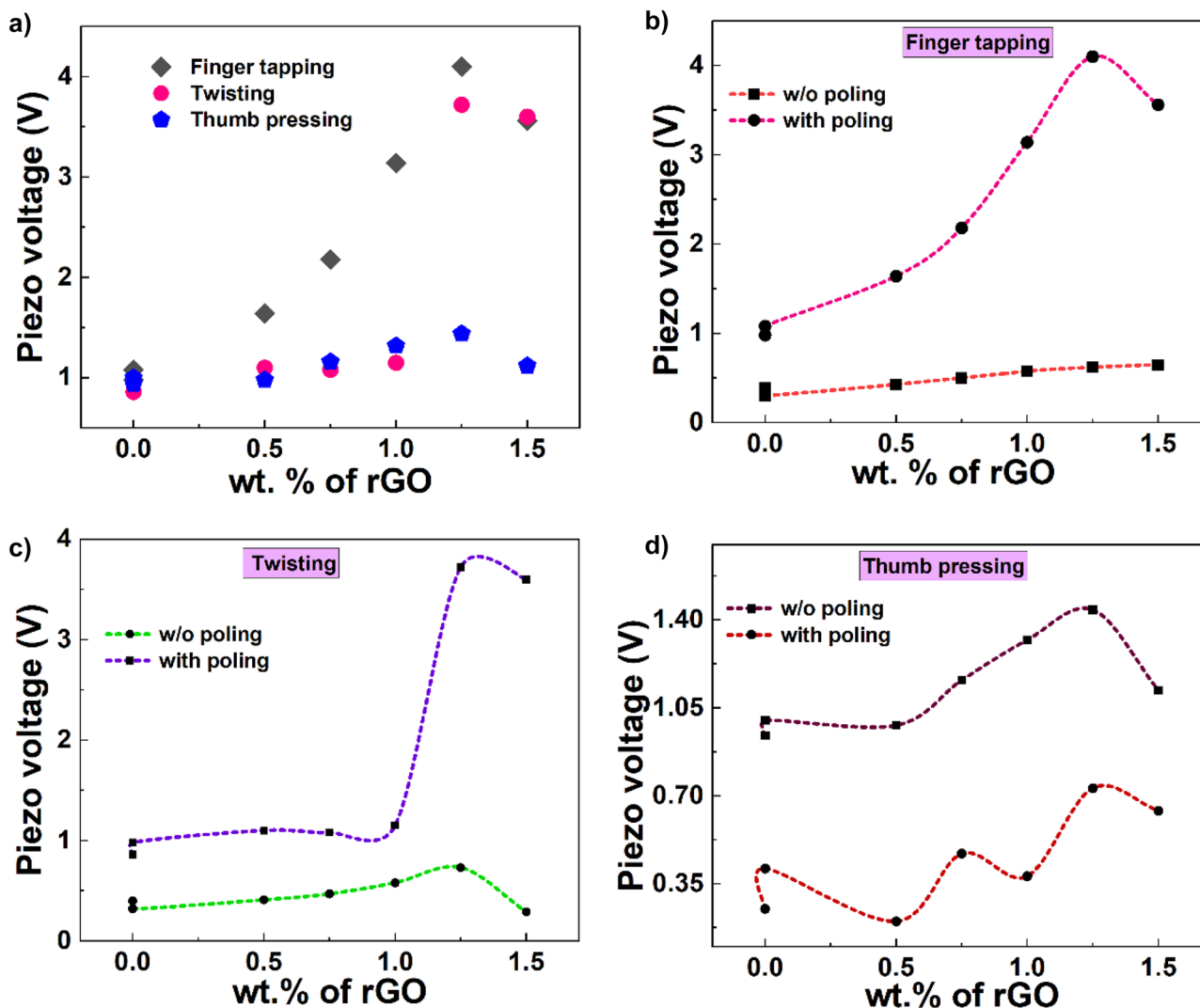


Fig. 15 Comparison of o/p voltage generated for nanocomposite samples **a** under different loading conditions, for poled and unpoled samples under **b** finger tapping condition, **c** twisting condition, **d** thumb pressing condition

Conclusion

This study illustrates the successful fabrication of a PVDF-BTO-rGO nanocomposite film with rGO loadings of 0, 0.5, 0.75, 1, 1.25 and 1.5 wt%. The piezoelectric behaviour of solvent cast PVDF-BTO-rGO nanocomposites were enhanced by subsequent electrode poling. A thorough analysis on the role of rGO concentration on thermal, mechanical, and piezoelectric properties of PVDF-BTO composites is conducted. XRD and FTIR studies confirmed the existence and enhancement of β phase of PVDF which is essential for piezoelectric behaviour. The values of Elastic modulus and tensile strength increased up to 1.25 wt% of rGO loading, followed by drastic reduction at higher loading. Sample ABC 1.25 displayed maximum viscosity and storage modulus as compared to pure PVDF. The dielectric constant and ac conductivity of

the nanocomposite samples are considerably improved on nanofiller addition. Piezo responses of poled and unpoled samples for different loading conditions were tested and compared. Electrode poled sample ABC 1.25 showed maximum V_{pp} value of 4.1 V for continuous finger tapping condition. The technique used in this work established the framework for the mass production of flexible PVDF-based films with improved mechanical properties and enhanced piezo response which has enormous potential in energy harvesting and structure health monitoring applications.

Acknowledgements This research work is supported by DST (grant no. TDP/BTD/03/2021(G)), India. The authors are grateful to the Central instrument facility (CIF), Indian Institute of technology Guwahati (IITG), for providing XRD characterization facilities. The authors wish to thank North East Centre for Biological Sciences and Healthcare Engineering (NECBH), IIT Guwahati and Department of

Biotechnology (DBT), Govt. of India for Project No. BT/COE/34/SP28408/2018 for the FESEM facility.

Funding This research work received funding from Department of Science & Technology (DST) under grant no. TDP/BDTD/03/2021(G) for “Development and testing of a wearable device for the early detection of a cartilage damage in a knee stepping towards an osteoarthritis condition using acoustic emission”.

Data Availability The datasets generated during and/or analyzed during the current study are available from the corresponding author upon reasonable request.

Declarations

Conflict of interest It is stated by the authors of this paper that they have no competing financial interests or interpersonal relationships that could have influenced their work in any way.

References

- Singh HH, Singh S, Khare N (2017) Design of flexible PVDF/NaNbO₃/RGO nanogenerator and understanding the role of nanofillers in the output voltage signal. *Compos Sci Technol* 149:127–133. <https://doi.org/10.1016/j.compscitech.2017.06.013>
- Li Y, Liao Y, Su Z (2018) Graphene-functionalized polymer composites for self-sensing of ultrasonic waves: an initiative towards “sensor-free” structural health monitoring. *Compos Sci Technol* 168:203–213. <https://doi.org/10.1016/J.COMPSCITECH.2018.09.021>
- Villa SM, Mazzola VM, Santaniello T et al (2019) Soft Piezoelectric/Piezoelectric Nanocomposites based on Ionogel/BaTiO₃ nanoparticles for low frequency and directional discriminative pressure sensing. *ACS Macro Lett* 8:414–420. <https://doi.org/10.1021/ACSMACROLETT.8B01011/ASSET>
- Ponnamma D, Parangusan H, Tanvir A, AlMa'adeed MAA (2019) Smart and robust electrospun fabrics of piezoelectric polymer nanocomposite for self-powering electronic textiles. *Mater Des* 184:108176. <https://doi.org/10.1016/J.MATDES.2019.108176>
- Ponnamma D, Chamakh MM, Deshmukh K et al (2017) Ceramic-based polymer nanocomposites as Piezoelectric materials. Springer, Cham, pp 77–93
- Jian G, Jiao Y, Meng Q et al (2021) Excellent high-temperature piezoelectric energy harvesting properties in flexible polyimide/3D PbTiO₃ flower composites. *Nano Energy* 82:105778. <https://doi.org/10.1016/J.NANOEN.2021.105778>
- Das S, Biswal AK, Parida K et al (2018) Electrical and mechanical behavior of PMN-PT/CNT based polymer composite film for energy harvesting. *Appl Surf Sci* 428:356–363. <https://doi.org/10.1016/J.APSUSC.2017.09.077>
- Dufay T, Guiffard B, Seveno R, Thomas J-C (2018) Energy Harvesting using a lead Zirconate Titanate (PZT) Thin Film on a polymer substrate. *Energy Technol* 6:917–921. <https://doi.org/10.1002/ente.201700732>
- Shi K, Sun B, Huang X, Jiang P (2018) Synergistic effect of graphene nanosheet and BaTiO₃ nanoparticles on performance enhancement of electrospun PVDF nanofiber mat for flexible piezoelectric nanogenerators. *Nano Energy* 52:153–162. <https://doi.org/10.1016/J.NANOEN.2018.07.053>
- Zhang B, Guo C, Cao X et al (2022) Flexoelectricity on the photovoltaic and pyroelectric effect and ferroelectric memory of 3D-printed BaTiO₃/PVDF nanocomposite. *Nano Energy* 104:107897. <https://doi.org/10.1016/J.NANOEN.2022.107897>
- Drakopoulos SX, Yang J, Vryonis O et al (2022) Flexible polymer-based nanodielectrics reinforced with electrospun composite nanofibers for capacitive energy storage. *ACS Appl Polym Mater*. <https://doi.org/10.1021/ACSAPM.2C01162/ASSET>
- Wang Z, Maruyama K, Narita F (2022) A novel manufacturing method and structural design of functionally graded piezoelectric composites for energy-harvesting. *Mater Des* 214:110371. <https://doi.org/10.1016/J.MATDES.2021.110371>
- Wan L, Tian W, Li N et al (2022) Hydrophilic porous PVDF membrane embedded with BaTiO₃ featuring controlled oxygen vacancies for piezocatalytic water cleaning. *Nano Energy* 94:106930. <https://doi.org/10.1016/J.NANOEN.2022.106930>
- Kumar M, Kulkarni ND, Kumari P (2022) Fabrication and characterization of PVDF/BaTiO₃ nanocomposite for energy harvesting application. *Mater Today Proc* 56:1151–1155. <https://doi.org/10.1016/J.MATPR.2021.11.133>
- Hazra S, Ghatak A, Ghosh A et al (2022) Enhanced piezoelectric response in BTO NWs-PVDF composite through tuning of polar phase content. *Nanotechnology* 34:045405. <https://doi.org/10.1088/1361-6528/AC9D41>
- Liu R, Liu Q, He D et al (2021) Enhancement of the piezoelectric property of polyvinylidene fluoride through electroactive phase enrichment and the application in piezoelectric generators. *ACS Appl Electron Mater* 3:1804–1812. <https://doi.org/10.1021/acsaelm.1c00074>
- Sukumaran S, Chatbourni S, Rouxel D et al (2021) Recent advances in flexible PVDF based piezoelectric polymer devices for energy harvesting applications. *J Intell Mater Syst Struct* 32:746–780. <https://doi.org/10.1177/1045389X20966058>
- Singh HH, Singh S, Khare N (2018) Enhanced β -phase in PVDF polymer nanocomposite and its application for nanogenerator. *Polym Adv Technol* 29:143–150. <https://doi.org/10.1002/pat.4096>
- Kulkarni ND, Kumari P (2023) Development of highly flexible PVDF-TiO₂ nanocomposites for piezoelectric nanogenerator applications. *Mater Res Bull* 157:112039. <https://doi.org/10.1016/j.materresbull.2022.112039>
- Dilip Kulkarni N, Kumar M, Kumari P (2022) PVDF/RGO based piezoelectric nanocomposite films for enhanced mechanical and dielectric properties. *Mater Today Proc*. <https://doi.org/10.1016/J.MATPR.2022.09.043>
- Yaqoob U, Chung GS (2017) Effect of surface treated MWCNTs and BaTiO₃ nanoparticles on the dielectric properties of a P(VDF-TrFE) matrix. *J Alloys Compd* 695:1231–1236. <https://doi.org/10.1016/J.JALLCOM.2016.10.250>
- Park K-I, Jeong CK, Kim NK, Lee KJ (2016) Stretchable piezoelectric nanocomposite generator. <https://doi.org/10.1186/s40580-016-0072-z>
- Li Y, Tan J, Liang K et al (2022) Enhanced piezoelectric performance of multi-layered flexible polyvinylidene fluoride–BaTiO₃–rGO films for monitoring human body motions. *J Mater Sci: Mater Electron* 33:4291–4304. <https://doi.org/10.1007/s10854-021-07622-7>
- Yaqoob U, Iftekhhar Uddin ASM, Chung GS (2016) The effect of reduced graphene oxide on the dielectric and ferroelectric properties of PVDF–BaTiO₃ nanocomposites. *RSC Adv* 6:30747–30754. <https://doi.org/10.1039/C6RA03155B>
- Yaqoob U, Chung GS (2017) Effect of reduced graphene oxide on the energy harvesting performance of P(VDF-TrFE)-BaTiO₃ nanocomposite devices. *Smart Mater Struct* 26. <https://doi.org/10.1088/1361-665X/aa81a0>
- Yaqoob U, Uddin ASMI, Chung GS (2017) A novel tri-layer flexible piezoelectric nanogenerator based on surface-modified graphene and PVDF–BaTiO₃ nanocomposites. *Appl Surf Sci* 405:420–426. <https://doi.org/10.1016/J.APSUSC.2017.01.314>
- Bakar EA, Mohamed MA, Ooi PC et al (2018) Fabrication of indium-tin-oxide free, all-solution-processed flexible nanogenerator device using nanocomposite of barium titanate and graphene quantum dots in polyvinylidene fluoride polymer matrix.

- Org Electron 61:289–295. <https://doi.org/10.1016/J.ORGEL.2018.06.006>
28. Luo J, Zhang L, Wu T et al (2021) Flexible electronic skin with high performance pressure sensing based on PVDF/rGO/BaTiO₃ composite thin film. *Org Electron* 98:106296. <https://doi.org/10.1016/J.ORGEL.2021.106296>
 29. Sharma R, Singh R, Batish A, Ranjan N (2021) On synergistic effect of BaTiO₃ and graphene reinforcement in polyvinylidene fluoride matrix for four dimensional applications. *Proc Inst Mech Eng C J Mech Eng Sci* 236:276–292. <https://doi.org/10.1177/09544062211015763>
 30. Sharma R, Singh R, Batish A On effect of chemical-assisted mechanical blending of barium titanate and graphene in PVDF for 3D printing applications. <https://doi.org/10.1177/0892705720945377>
 31. Nikiforov M, Liu H, Craighead H, Bonnell D (2006) Polarization controlled transport in PANI–BaTiO₃ nanofibers. *Nano Lett* 6:896–900. <https://doi.org/10.1021/nl052017r>
 32. Arunguvai J, Lakshmi P (2020) Flexible nano-vibration energy harvester using three-phase polymer composites. *J Mater Sci: Mater Electron* 31:8283–8290. <https://doi.org/10.1007/S10854-020-03363-1/TABLES/2>
 33. Hayashi H, Nakamura T, Ebina T (2013) In-situ Raman spectroscopy of BaTiO₃ particles for tetragonal–cubic transformation. *J Phys Chem Solids* 74:957–962. <https://doi.org/10.1016/J.JPCS.2013.02.010>
 34. Kaspar P, Sobola D, Částková K et al (2021) Case study of polyvinylidene fluoride doping by carbon nanotubes. *Materials* 14. <https://doi.org/10.3390/MA14061428>
 35. Cai X, Lei T, Sun D, Lin L (2017) A critical analysis of the α , β and γ phases in poly(vinylidene fluoride) using FTIR. *RSC Adv* 7:15382–15389. <https://doi.org/10.1039/C7RA01267E>
 36. Kim S, Song Y, Heller MJ (2017) Influence of MWCNTs on β -Phase PVDF and triboelectric properties. *J Nanomater* 2017. <https://doi.org/10.1155/2017/2697382>
 37. Naik R, Somasekhara Rao T (2019) Self-powered flexible piezoelectric nanogenerator made of poly (vinylidene fluoride)/Zirconium oxide nanocomposite. *Mater Res Express* 6. <https://doi.org/10.1088/2053-1591/ab49b3>
 38. Kumar M, Kumari P (2022) P(VDF-TrFE)/ZnO nanocomposite synthesized by electrospinning: effect of ZnO nanofiller on physical, mechanical, thermal, rheological and piezoelectric properties. *Polym Bull* 1–20. <https://doi.org/10.1007/S00289-022-04275-2/TABLES/3>
 39. Shepelin NA, Glushenkov AM, Lussini VC et al (2019) New developments in composites, copolymer technologies and processing techniques for flexible fluoropolymer piezoelectric generators for efficient energy harvesting. *Energy Environ Sci* 12:1143–1176. <https://doi.org/10.1039/C8EE03006E>
 40. Anand A, Meena D, Dey KK, Bhatnagar MC (2020) Enhanced piezoelectricity properties of reduced graphene oxide (RGO) loaded polyvinylidene fluoride (PVDF) nanocomposite films for nanogenerator application. *J Polym Res* 27:1–11. <https://doi.org/10.1007/S10965-020-02323-X/FIGURES/10>
 41. Gyan DS, Dwivedi A (2019) Structural and electrical characterization of NaNbO₃-PVDF nanocomposites fabricated using cold sintering synthesis route. *J Appl Phys* 125:024103. <https://doi.org/10.1063/1.5046458>
 42. Zeyrek Ongun M, Oguzlar S, Doluel EC et al (2020) Enhancement of piezoelectric energy-harvesting capacity of electrospun β -PVDF nanogenerators by adding GO and rGO. *J Mater Sci: Mater Electron* 31:1960–1968. <https://doi.org/10.1007/s10854-019-02715-w>
 43. Layek RK, Samanta S, Chatterjee DP, Nandi AK (2010) Physical and mechanical properties of poly(methyl methacrylate)-functionalized graphene/poly(vinylidene fluoride) nanocomposites: piezoelectric β polymorph formation. *Polym (Guildf)* 51:5846–5856. <https://doi.org/10.1016/j.polymer.2010.09.067>
 44. Benz M, Euler WB (2003) Determination of the crystalline phases of poly(vinylidene fluoride) under different preparation conditions using differential scanning calorimetry and infrared spectroscopy. *J Appl Polym Sci* 89:1093–1100. <https://doi.org/10.1002/APP.12267>
 45. Karan SK, Mandal D, Khatua BB (2015) Self-powered flexible Fe-doped RGO/PVDF nanocomposite: an excellent material for a piezoelectric energy harvester. *Nanoscale* 7:10655–10666. <https://doi.org/10.1039/C5NR02067K>
 46. Chiu FC (2014) Comparisons of phase morphology and physical properties of PVDF nanocomposites filled with organoclay and/or multi-walled carbon nanotubes. *Mater Chem Phys* 143:681–692. <https://doi.org/10.1016/J.MATCHEMPHYS.2013.09.054>
 47. Li W, Dichiara A, Bai J (2013) Carbon nanotube–graphene nanoplatelet hybrids as high-performance multifunctional reinforcements in epoxy composites. *Compos Sci Technol* 74:221–227. <https://doi.org/10.1016/J.COMPSCITECH.2012.11.015>
 48. Sharma R, Singh R, Batish A (2019) Study on barium titanate and graphene reinforced PVDF matrix for 4D applications. *J Thermoplast Compos Mater* 34:1234–1253. <https://doi.org/10.1177/0892705719865004>
 49. Zhang H, Zhao M, Huang ZX, Qu JP (2020) Synergistic Effect based on enhanced local shear forces in PVDF/TiO₂/CNT ternary composites. *Ind Eng Chem Res* 59:18887–18897
 50. Kumar M, Kumari P, Sahatiya P (2022) P(VDF-TrFE)/ZnO nanofiber composite based piezoelectric nanogenerator as self-powered sensor: fabrication and characterization. *J Polym Res* 29:1–16. <https://doi.org/10.1007/S10965-022-02890-1/TABLES/5>
 51. Zhang Y, Zuo M, Song Y et al (2015) Dynamic rheology and dielectric relaxation of poly(vinylidene fluoride)/poly(methyl methacrylate) blends. *Compos Sci Technol* 106:39–46. <https://doi.org/10.1016/J.COMPSCITECH.2014.10.024>
 52. Ponnamma D, Goutham S, Sadasivuni KK et al (2018) Controlling the sensing performance of rGO filled PVDF nanocomposite with the addition of secondary nanofillers. *Synth Met* 243:34–43. <https://doi.org/10.1016/j.synthmet.2018.05.014>
 53. Shokrieh MM, Hosseinkhani MR, Naimi-Jamal MR, Tourani H (2013) Nanoindentation and nanoscratch investigations on graphene-based nanocomposites. *Polym Test* 32:45–51. <https://doi.org/10.1016/J.POLYMERTESTING.2012.09.001>
 54. Wang J, Yi M, Shen Z et al (2019) Enhanced thermal and mechanical properties of poly (vinylidene fluoride) nanocomposites reinforced by liquid-exfoliated graphene. *J Macromol Sci A* 56:733–740. <https://doi.org/10.1080/10601325.2019.1607375>
 55. Yang J, Zhang Z, Friedrich K, Schlarb AK (2007) Creep resistant polymer nanocomposites reinforced with multiwalled carbon nanotubes. *Macromol Rapid Commun* 28:955–961. <https://doi.org/10.1002/MARC.200600866>
 56. Luo B, Wang X, Wang Y, Li L (2014) Fabrication, characterization, properties and theoretical analysis of ceramic/PVDF composite flexible films with high dielectric constant and low dielectric loss. *J Mater Chem A Mater* 2:510–519. <https://doi.org/10.1039/c3ta14107a>

Publisher's note Springer Nature remains neutral with regard to jurisdictional claims in published maps and institutional affiliations.

Springer Nature or its licensor (e.g. a society or other partner) holds exclusive rights to this article under a publishing agreement with the author(s) or other rightsholder(s); author self-archiving of the accepted manuscript version of this article is solely governed by the terms of such publishing agreement and applicable law.